A modified two-stage isolated bidirectional buck-DAB converter with a full-load ZVS range

Jinliang Li[1,2], Dai Wan[1,2], Zhengmei Lu[3]* and Guo Xu[3]

[1]State Grid Hunan Electric Power Company Limited Research Institute, Changsha, China, [2]State Grid Joint Laboratory for Intelligent Application and Key Equipment in Distribution Network Institute, Changsha, China, [3]School of Automation, Central South University, Changsha, China

A modified two-stage buck-DAB (MBDAB) converter is proposed to improve the performance of the traditional two-stage buck-DAB (TSBDAB) converter. In the MBDAB converter, the DAB can work with fixed voltage gain and voltage-matched condition under a wide input voltage range. The voltage gain of the converter is adjusted through the added front-end stage, which is similar to a buck converter. Compared with the TSBDAB converter, only part of the transmitted power flows through the front-end stage, so the loss of the buck stage and the burden of zero-voltage switching (ZVS) can be reduced. Detailed analysis of the working principle, partial power characteristics, and the full-load ZVS range design are presented. To verify the effectiveness of the proposed MBDAB converter, experimental results are obtained from a prototype with a rated power of 1 kW.

KEYWORDS

isolated DC/DC converter, modified two-stage, buck-DAB converter, zero-voltage switching, bidirectional converter

1 Introduction

Bidirectional DC/DC converters play a crucial role in various applications like DC microgrids and energy storage systems to provide electrical isolation and voltage gain regulation capability (Inoue and Akagi, 2007; Masrur et al., 2018; Tu et al., 2019). In the domain of traditional IBDC converters, there are two key types: resonant converters and dual active bridge (DAB) converters (Zhao et al., 2014). DAB converters have gained significant interest due to their numerous benefits, such as electrical isolation, high efficiency, the ability to transfer energy bidirectionally, and soft-switching characteristics (Shao et al., 2019).

The single phase shift (SPS) control has only one degree of freedom, which is very simple (Doncker et al., 1988). However, the efficiency of the SPS-controlled DAB converter is low when the voltage gain is far away from the unity gain due to the large current stress and backflow power, and the zero-voltage switching (ZVS) cannot be achieved under full range. Therefore, to improve the efficiency of the DAB converter under a wide voltage range, modulation strategies with more control variables have been proposed. Extended phase shift (EPS) control and dual phase shift (DPS) control are two common two-degree-of-freedom control methods (Zhao et al., 2012; Sun et al., 2020). An inner phase-shift angle is introduced to reduce the RMS inductance current and the backflow power under a wide voltage range. Triple phase shift (TPS) control (Everts, 2017; Guo, 2020) is designed to further improve the performance of the DAB. There are three degrees of freedom in TPS control, which results in increased
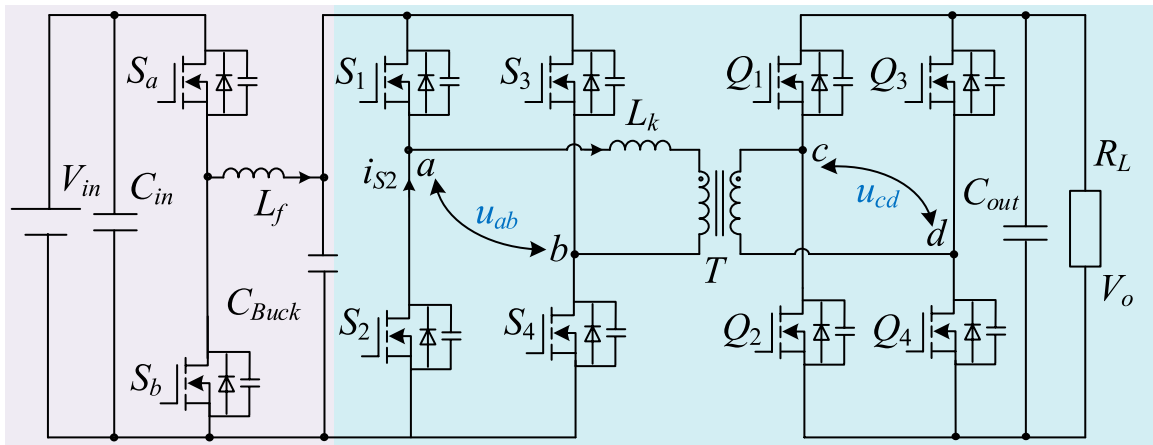
FIGURE 1
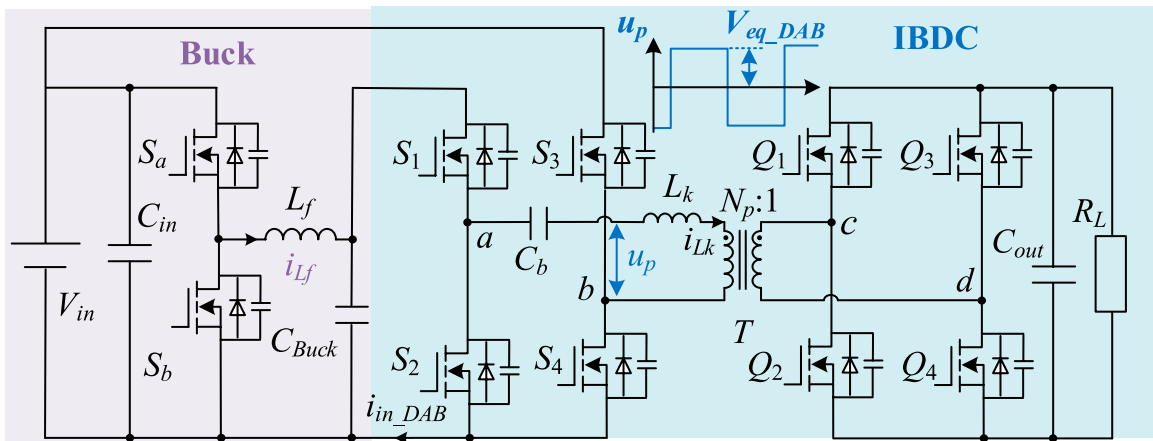Topology of the TSBDAB converter.

FIGURE 2
Topology of the proposed MBDAB converter.

complexity in both the operation modes and control strategy due to the added degree of freedom.

Another effective and simple solution for improving the performance of the converter under a wide voltage range is the restructuring of its topology (Alou et al., 2001; Lee et al., 2011; Fu et al., 2020; Xu et al., 2020; Liao et al., 2022; Lin et al., 2022). The core concept of this technique is to enable the DAB converter to operate under a unity gain condition across a wide voltage range by restructuring the topology. One straightforward way is the two-stage cascade solution. To achieve high performance, the IBDC converter operates under fixed voltage gain in the two-stage cascade scheme. The two-stage structure includes two DC/DC converters, and one of them has isolation properties, as detailed in Alou et al. (2001), Lee et al. (2011), Fu et al. (2020), and Xu et al. (2020). Figure 1 illustrates the configuration of the TSBDAB converter. Fu et al. (2020) enhanced the efficiency by combining the IBDC converter with a non-isolated boost converter. ZVS of all switches is
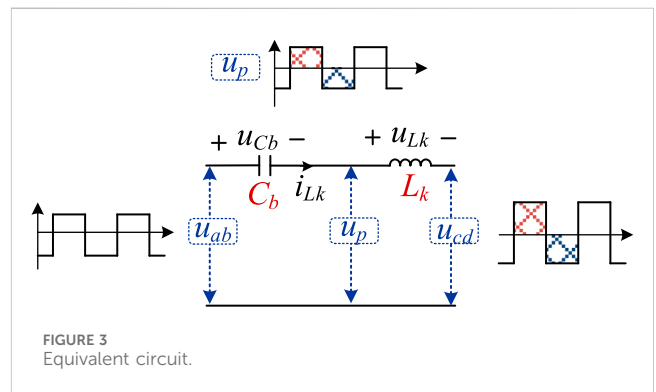

FIGURE 3
Equivalent circuit.

achieved, and the overall losses are reduced. Xu et al. (2020) combined a DAB converter and a buck–boost converter to achieve superior performance under a wide voltage gain range. Lin et al. (2022) described the combination of the DAB and the
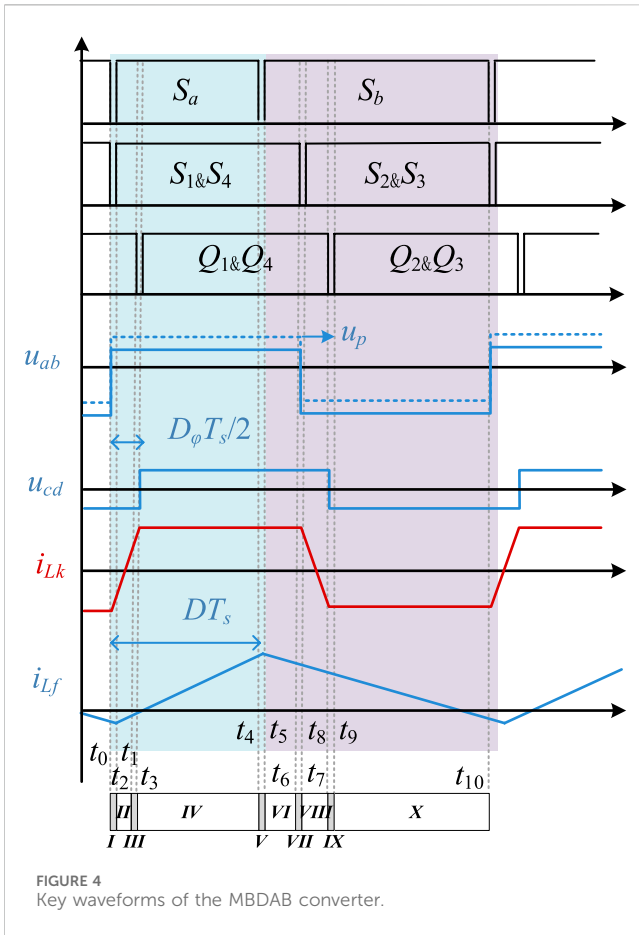
FIGURE 4
Key waveforms of the MBDAB converter.

boost converter in input-series configuration. High efficiency can be achieved by power-sharing adjustments between the two converters.

All of the power should be transferred by the front-end stage in the existing two-stage scheme, which leads to increased conversion loss. To improve the efficiency of the two-stage scheme and reduce the front-end-stage-transferred power, a partial power converter (PPC) approach as mentioned in Sun et al. (2008), Zientarski et al. (2019), and Liao et al. (2022) can be used. The PPC concept involves integrating the PPC submodule alongside the main power converters, either in parallel or in series. It is important to note that the PPC solution typically does not provide electrical isolation, as it often uses buck or buck/boost converters for the DC–DC conversion with partial power characteristics, as explained in Sun et al. (2008).

In this article, a modified isolated bidirectional buck-DAB converter is proposed to construct partial power transmission characteristics of the front-stage converter and further improve the efficiency of the two-stage converter under a wide voltage range. The proposed converter only requires a simple change in the connection architecture of the TSBDAB converter. In the MBDAB converter, when the input voltage changes, the front-end buck stage performs a gain adjustment, whereas DAB operates under a fixed voltage gain condition. In addition, the buck stage can only transmit part of the output power, which is due to the change in the connection architecture of the TSBDAB

scheme. All the switches of the proposed converter can achieve the ZVS operation.

2 Proposed MBDAB converter and operation principles

2.1 Proposed modified buck-DAB converter

Figure 2 illustrates the proposed MBDAB converter. Compared with the TSBDAB converter in Figure 1, to achieve the partial power conversion, the source of S_1 is disconnected from the source of S_3, and the source of S_3 is directly connected to the input voltage. In addition, a blocking capacitor C_b is added to ensure that the voltages on both sides of the leakage inductor L_k are matched. The buck stage consists of two switches ($S_{a\text{-}b}$), an inductor (L_f), and a capacitor (C_{Buck}). The DAB stage consists of two full bridges in the primary side and the secondary side, connected by a high-frequency transformer T with the turns ratio of N_p:1, an inductor (L_k), and a capacitor (C_b).

2.2 Mechanism of DC block capacitor C_b

The equivalent circuit of the DAB stage is shown in Figure 3. When the DAB stage is under the SPS control, the voltages on both sides of the leakage inductor are in volt–second equilibrium, which ensures that the inductor current i_{Lk} does not diverge. According to Figure 3, the relationship can be calculated as Eq. 1:

$$L_k \frac{d\bar{i}_{Lk}}{dt} = \bar{u}_{Lk} = \bar{u}_{ab} - \bar{u}_{cb} - \bar{u}_{cd}. \tag{1}$$

The steady state of the converter means that the average voltage of inductor L_k is 0. The relationship between the u_{ab}, u_p and u_{cd} is shown in Figure 3, the average values of u_{cd} and u_{ab} are 0 and $(V_{in}-V_{Buck})/2$, then the voltage on DC block capacitor C_b can be deduced as Eq. 2:

$$|\bar{u}_{cb}| = |\bar{u}_{ab}| = \frac{V_{in} - V_{Buck}}{2}. \tag{2}$$

2.3 Modulation strategies and operation principles

Figure 4 illustrates the modulation strategy and theoretical operating waveforms of the proposed MBDAB converter. According to Figure 4, switches S_a and S_b are driven complementarily, and pulse width modulation is applied to the buck converter. As for the DAB stage, the conventional SPS modulation is applied. It is very simple with a fixed 50% duty ratio.

The duty cycle D of S_a is to regulate the voltage across C_{Buck}. The half-cycle phase shift ratio D_{φ} is used to regulate the output power of
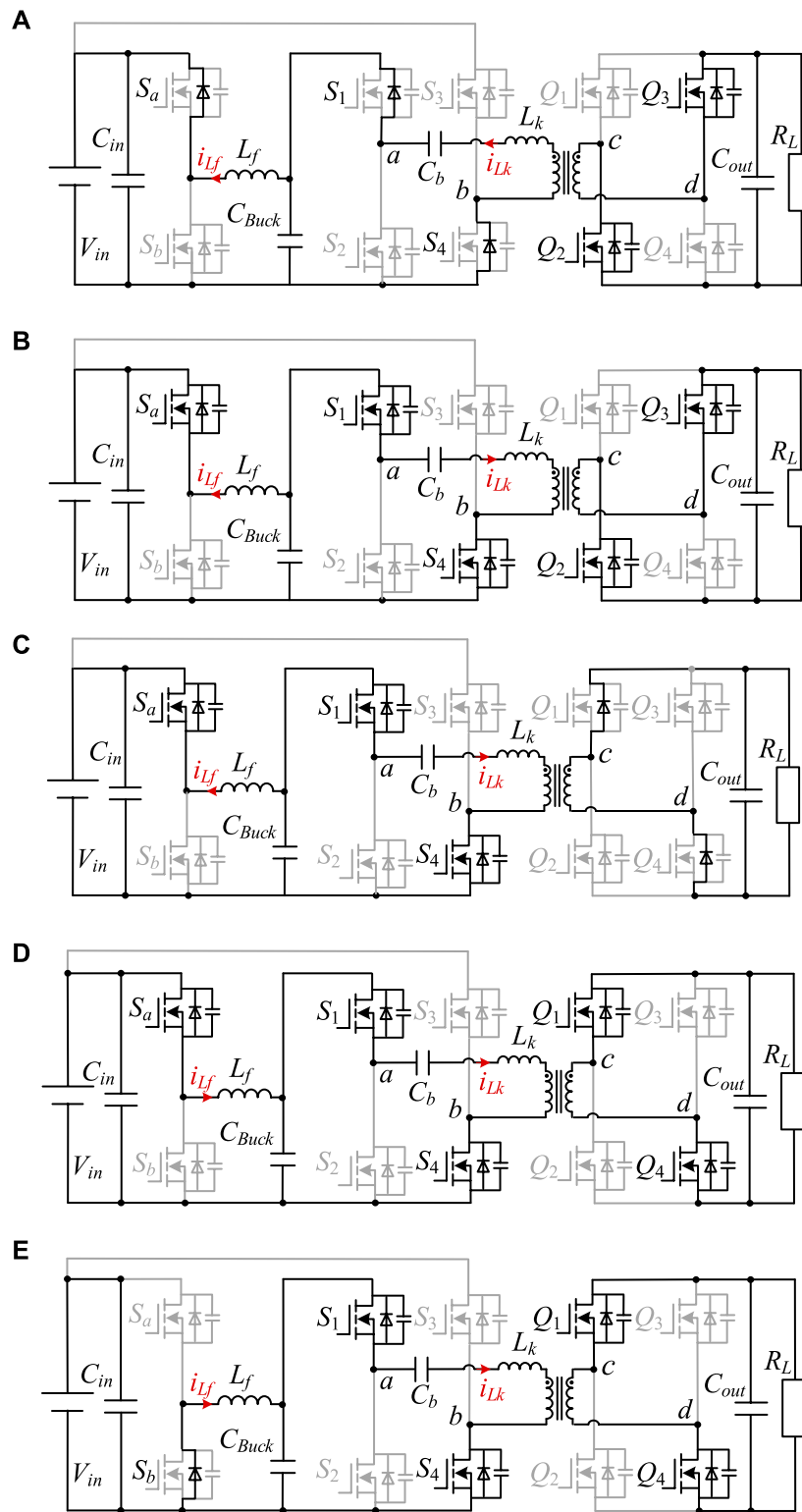
FIGURE 5
(Continued).
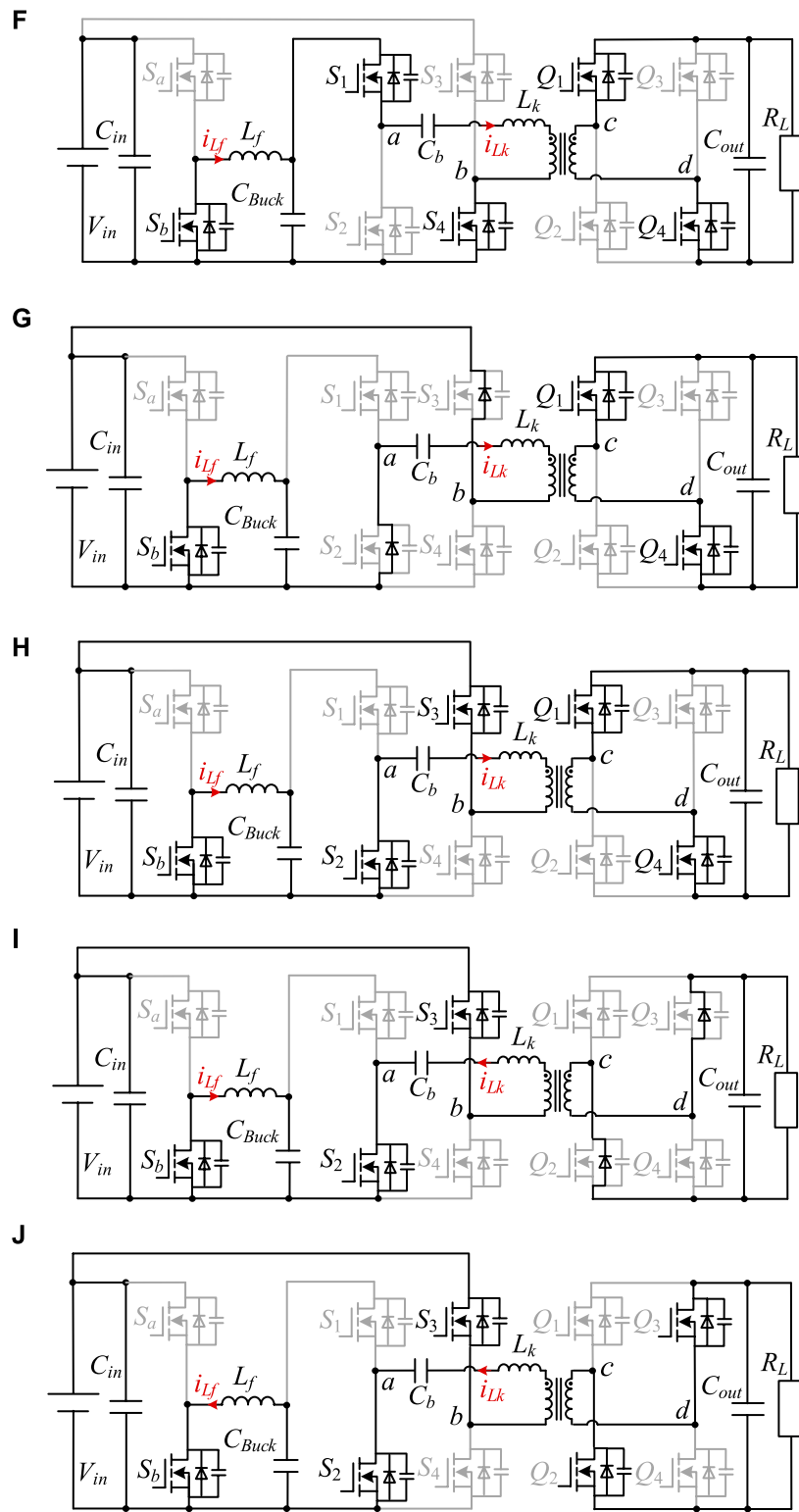
FIGURE 5
(Continued). Operational principles of the proposed converter: **(A)** *stage I* (t_0–t_1); **(B)** *stage II* (t_1–t_2); **(C)** *stage III* (t_2–t_3); **(D)** *stage IV* (t_3–t_4); **(E)** *stage V* (t_4–t_5); **(F)** *stage VI* (t_5–t_6); **(G)** *stage VII* (t_6–t_7); **(H)** *stage VIII* (t_7–t_8); **(I)** *stage IX* (t_8–t_9); and **(J)** *stage X* (t_9–t_{10}).

FIGURE 6
Control diagram of the proposed MBDAB converter.
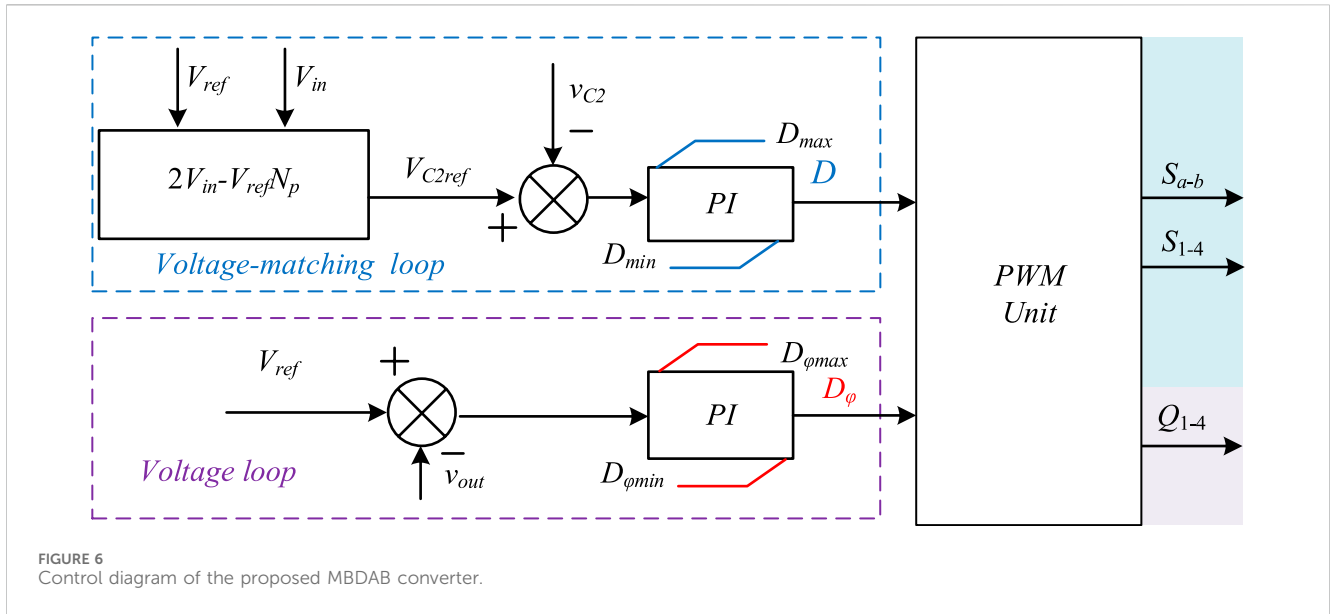
TABLE 1 Specific parameters.

| Parameter	Value
V_{in}	250–450 V
V_o	48 V
V_{eq_DAB}	240 V
N_p:1	5:1
L_k	39 μH
P	1,000 W
fs	100 kHz
C_{Buck}	25 μF
C_{in}/C_{out}	250 μF

DAB. It is worth pointing out that S_a and S_1 do not have to be turned on at the same time.

The 10 operating intervals are analyzed as follows and shown in Figure 5.

Stage I (t_0–t_1): At t_0, switches S_b, S_2, and S_3 are turned off. During stage I, since the currents i_{Lf} and i_{Lk} are negative, respectively, the body diodes of S_a, S_1, and S_4 are turned on. The conduction of diodes provides the conditions for the ZVS of the corresponding switches.

Stage II (t_1–t_2): At t_1, switches S_a, S_1, and S_4 are turned on under the ZVS condition. The voltage across inductors L_f and L_k is kept constant, and the currents i_{Lf} and i_{Lk} increase linearly. The inductor currents i_{Lf} and i_{Lk} are expressed in Eqs 3, 4:

$$L_f \frac{di_{Lf}}{dt} = V_{in} - DV_{in},$$ (3)

FIGURE 7
Prototype of the proposed MBDAB converter.
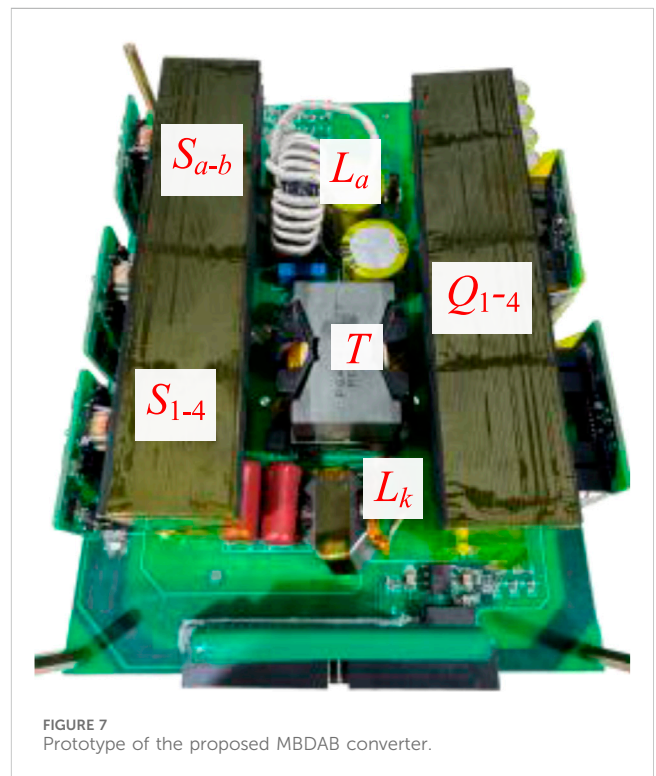
$$L_k \frac{di_{Lk}}{dt} = \frac{V_{in}(1+D)}{dt} = N_P + V_O.$$ (4)

Stage III (t_2–t_3): At t_2, switches Q_2 and Q_3 are turned off. During stage III, since the current i_{Lk} is positive, the body diodes of Q_1 and Q_4 are turned on. The conduction of diodes provides the conditions for the ZVS of the corresponding switches.

FIGURE 8
Steady-state waveforms of **(A)** V_{in} = 250 V; **(B)** V_{in} = 450 V.

Stage IV (t_3–t_4): At t_3, switches Q_1 and Q_4 are turned on under the ZVS condition. Since the voltage across the inductor Lk is zero under the voltage-matching condition, i_{Lk} keeps constant.

Stage V (t_4–t_5): At t_4, the switch S_a is turned off. Since the inductor current i_{Lf} is positive during stage V, the body diodes of S_b are turned on, which provides the conditions for ZVS of S_b.

Stage VI (t_5–t_6): At t_5, the switch S_b is turned on under the ZVS condition. The voltage across the inductor L_f is kept constant, and the current i_{Lf} decreases linearly which is expressed in Eq. 5:

$$L_f \frac{di_{Lf}}{dt} = -DV_{in}. \tag{5}$$

Stage VIII (t_7–t_8): At t_7, switches S_2 and S_3 are turned on under the ZVS condition. The voltage across the inductor L_k is kept constant, and the current i_{Lk} decreases linearly, which is expressed in Eq. 6:

$$L_k \frac{di_{Lk}}{dt} = -\frac{V_{in}(1+D)}{dt} = N_P V_O. \tag{6}$$

Stage IX (t_8–t_9): At t_8, switches Q_1 and Q_4 are turned off. During stage IX, since the current i_{Lk} is negative, the body diodes of Q_2

and Q_3 are turned on. The conduction of diodes provides the conditions for the ZVS of the corresponding switches.
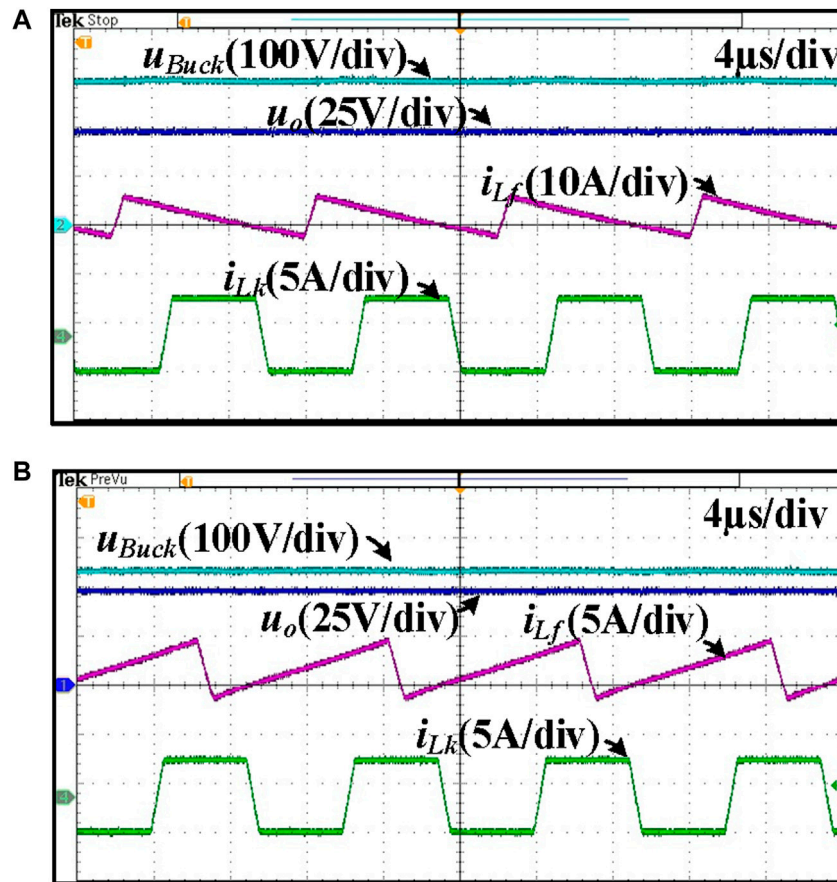
Stage X (t_9–t_{10}): At t_9, switches Q_2 and Q_3 are turned on under the ZVS condition. Since the voltage across the inductor L_k is zero under the voltage-matching condition, the current i_{Lk} keeps constant.

3 Steady-state analysis of the proposed MBDAB converter

3.1 Analysis of the voltage gain ratio of the MBDAB converter

Under the SPS modulation strategy, the output power of DAB in the MBDAB converter can be expressed as Eq. 7:

$$P_{out} = \frac{N_p V_{eq} V_{out} D_{\varphi}(1 - D_{\varphi})}{2L_k f_s}, \tag{7}$$

where N_p is the ratio of the high-frequency transformer and fs is the switching frequency of the converter. V_{eq} is one half of the peak-to-peak value of the voltage u_p, which can also be regarded as the
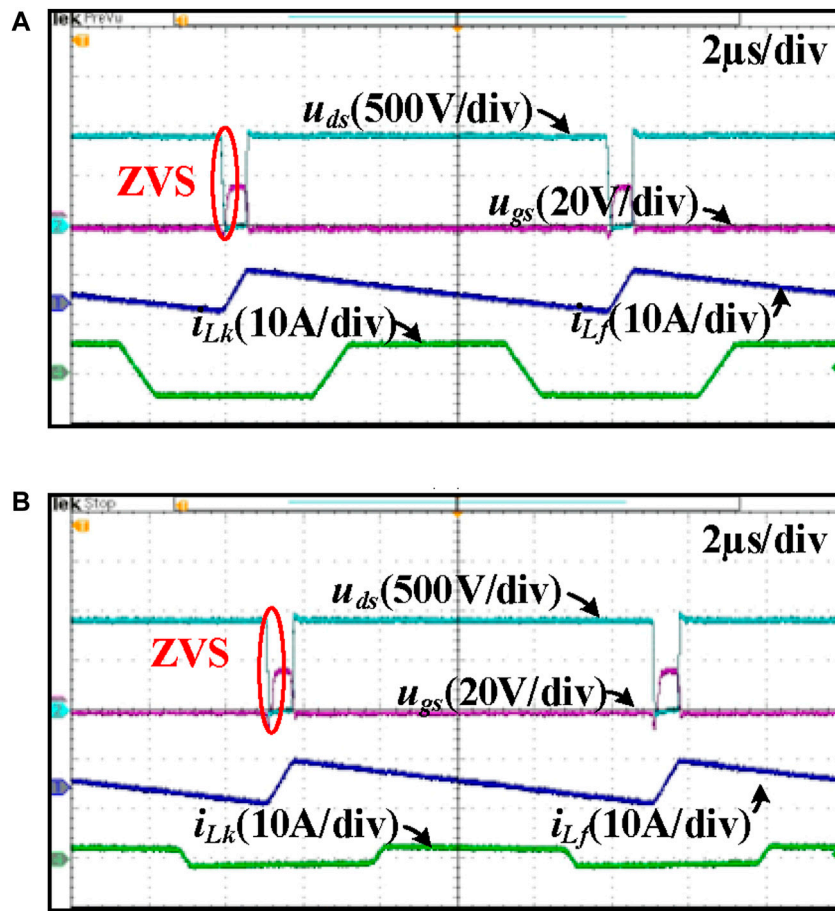
FIGURE 9
ZVS waveforms of S_a when V_{in} = 250 V: **(A)** light load; **(B)** heavy load.

equivalent input voltage of DAB. The expression of V_{eq} can be deduced as Eq. 8:

$$V_{eq} = \frac{V_{in} + V_{Buck}}{2}.$$
(8)

Therefore, the voltage gain of the DAB circuit in the modified buck-DAB converter can be derived as follows:

$$P_{out} = \frac{N_P V_{eq} V_{out} D_\varphi (1 - D_\varphi)}{2 L_k f_s} = \frac{V_{out}^2}{R_L},$$

$$\Rightarrow M_1 = \frac{V_{out}}{V_{eq}} = \frac{N_P D_\varphi (1 - D_\varphi) R_L}{2 L_k f_s}$$
(9)

where R_L is the resistance value of the load resistance and M_1 is the voltage gain of the DAB circuit. In order to achieve the voltage-matched condition of the DAB primary and secondary sides, the normalized gain of DAB is controlled to be constant at 1 in this converter, that is, $N_P M_1 = 1$.

The voltage gain of the buck circuit is expressed as Eq. 10:

$$\frac{V_{Buck}}{V_{in}} = D.$$
(10)

Considering the voltage gain of the buck part yields Eq. 11:

$$M_2 = \frac{V_{eq}}{V_{in}} = \frac{1 + D}{2}.$$
(11)

The voltage gain of the MBDAB converter can be expressed as Eq. 12:

$$M = M_1 M_2 = \frac{V_{out}}{V_{in}} = \frac{1 + D}{2 N_P}.$$
(12)

It can be known from Eq. 9 that the voltage gain ratio is related to D of the buck stage and N_P. When D is within the range of [0,1], the normalized voltage gain ratio (MN_P) is within the range of [0.5,1].

3.2 Transferred power of the buck stage

In the proposed MBDAB converter, the buck stage only transfers power when S_1 is on, so the transferred power of it is always smaller than the output power of the system. In addition, the power is directly transferred from the input voltage V_{in} when the switch S_3 is on. Then, the inductor current of the buck stage has a smaller offset
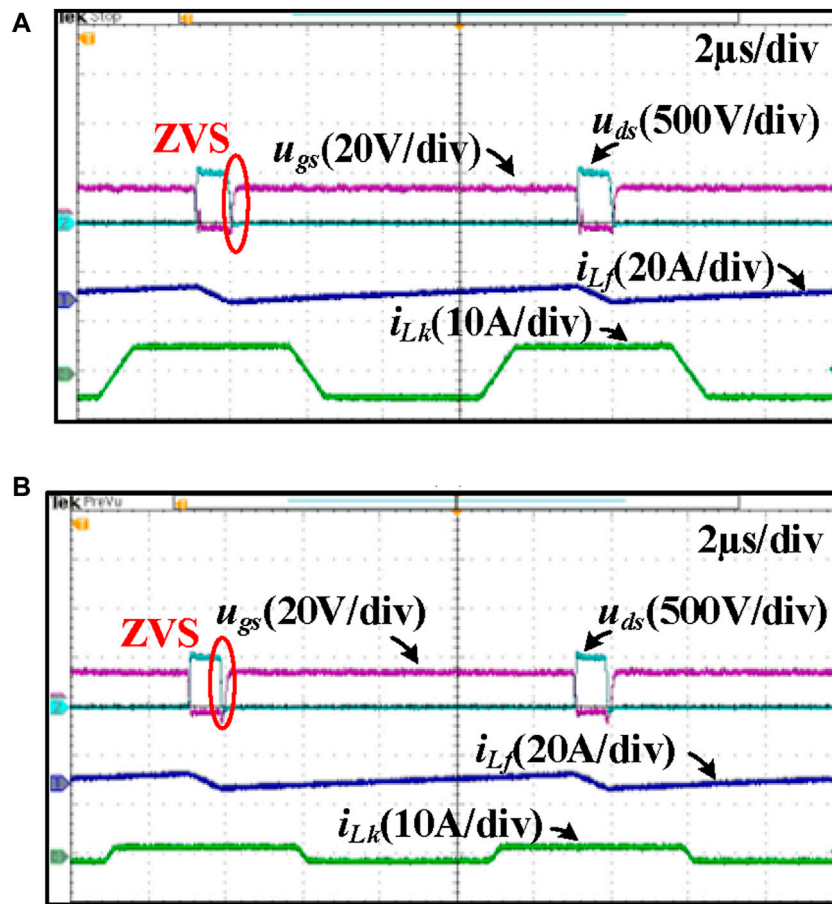
FIGURE 10
ZVS waveforms of S_a when V_{in} = 450 V: **(A)** light load; **(B)** heavy load.

and RMS value. It will reduce the loss and size of the buck inductor and help meet the ZVS condition of the buck switches.

The power of the MBDAB converter can be expressed as Eq. 13, according to power transmission characteristics of the DAB stage.

$$P = \frac{N_p V_{eq\_DAB} V_o D_\varphi (1 - D_\varphi)}{L_k f_s}. \tag{13}$$

Because the average inductor current is equal to half of the average DAB stage input current, the load current of the buck circuit can be expressed as Eq. 14:

$$i_{Load\_Buck} = \frac{1}{2} i_{in\_DAB} = \frac{N_p V_o D_\varphi (1 - D_\varphi)}{2 L_k f_s}. \tag{14}$$

The transferred power of the buck stage can be expressed as Eq. 15:

$$P_{Buck} = V_{buck} i_{Load\_Buck=} = \frac{N_p V_o D_\varphi (1 - D_\varphi) D V_{in}}{4 L_k f_s}. \tag{15}$$

The power transfer ratio for the buck stage to the DAB stage can be expressed as Eq. 16:

$$\frac{P_{Buck}}{P} = \frac{D}{1 + D} \leq 1. \tag{16}$$

3.3 Analysis of the ZVS condition

First, the ZVS conditions of the DAB circuit are analyzed. It can be seen from Figure 4 that before the switches S_1 and S_4 are turned on, the inductor current $i_{Lk} < 0$ should be ensured to discharge the junction capacitor of the switches and make their body diodes turn on. Before the switches Q_1 and Q_4 are turned on, the inductor current $i_{Lk} > 0$ should be ensured. The situation is similar when switches S_{2-3} and Q_{2-3} are switched on.

Therefore, the conditions for all switches of the DAB circuit to realize ZVS can be summarized as Eq. 17:

$$\begin{cases} i_{Lk}(t_1) < 0, \\ i_{Lk}(t_3) > 0. \end{cases} \tag{17}$$

To simplify the calculation, the change in the current in the dead time is ignored in the deduction. According to Formulas 4, 6 and the voltage-matching condition, the leakage inductor current at times t_1 and t_3 in the modified buck-DAB converter can be obtained as Eqs 18, 19:

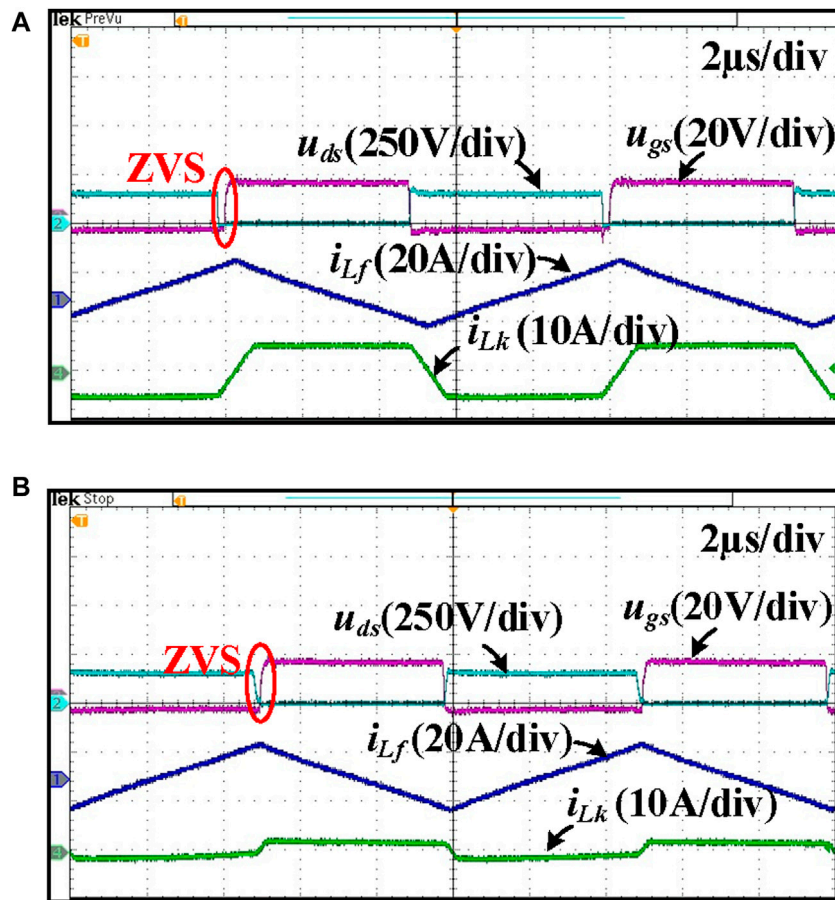$$i_{Lk}(t_1) = \frac{D_\varphi N_p v_{out}}{2 L_k f_s}, \tag{18}$$

FIGURE 11
ZVS waveforms of S_1 under **(A)** light load; **(B)** heavy load.

$$i_{Lk}(t_3) = -\frac{D_\varphi N_p v_{out}}{2L_k f_s}. \tag{19}$$

It can be seen from the equation that when the modified buck-DAB satisfies the voltage-matched conditions, all switches in the DAB circuit can achieve the ZVS condition under any voltage gain and any load conditions.

As for the buck stage, the polarity of i_{Lf} before S_a and S_b are turned on determines the ZVS realization. The ZVS can always be achieved for S_a since $i_{Lf}(t) < 0$ are always feasible. By properly designing the inductance value of L_f, $i_{Lf}(t_2)<0$ can be ensured. Then, S_b can achieve ZVS turn on. The condition of S_b to realize ZVS turn on is shown in Eq. 20:

$$\frac{P}{V_{in}(D+1)} - \frac{D(1-D)V_{in}}{2f_s L_f} < 0. \tag{20}$$

3.4 Control strategy of the MBDAB converter

Based on the voltage-matched principle, the converter control strategy is designed as follows. The control block diagram is shown in Figure 6. The converter has two control degrees of freedom, D and D_φ, which are the output of the voltage-matching control loop and the output of the voltage-regulating loop, respectively. In the voltage control loop, the direction of the output voltage and transmission power is changed by adjusting the phase shift ratio D_φ.

4 Experimental verifications

To validate the effectiveness of the proposed MBDAB converter, a 1-kW prototype is designed. The main parameters of the prototype are presented in Table 1. In addition, the prototype of the MBDAB converter is shown in Figure 7.

The steady-state experimental waveforms of the MBDAB converter under V_{in} = 250 V and V_{in} = 450 V are shown in Figure 8. The voltage across the auxiliary capacitor C_{Buck}, the output voltage of the MBDAB converter, the buck inductor current i_{Lf}, and the DAB leakage inductor current are shown in the figure. As can be seen, the output voltage of the MBDAB converter can be stabilized at 48 V. The DAB leakage
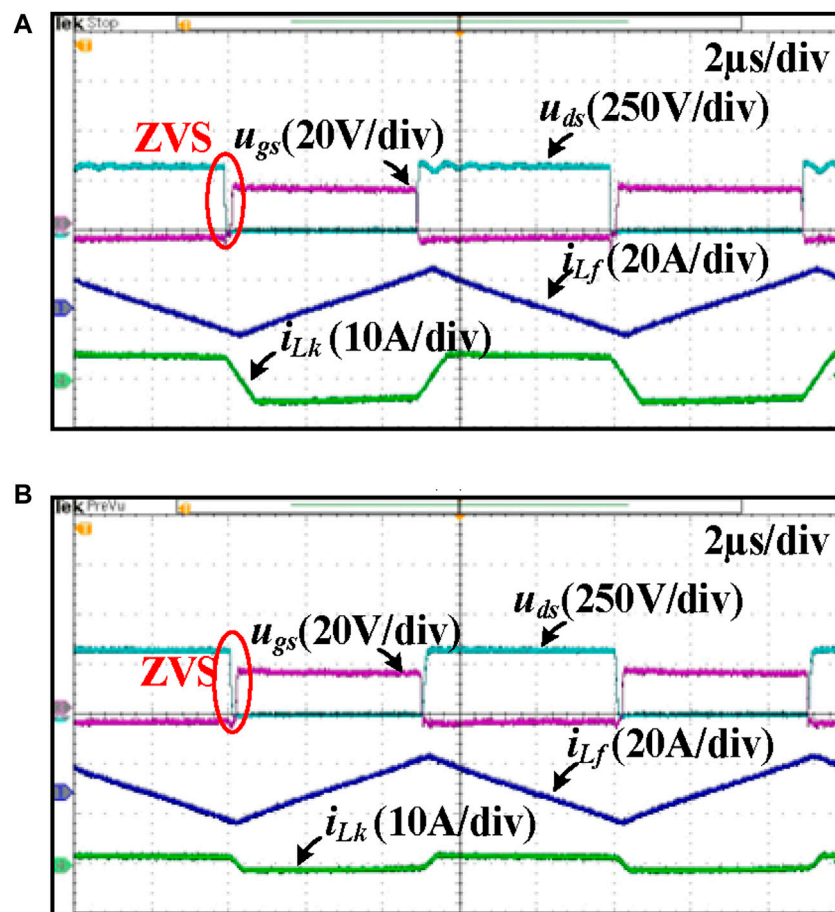
FIGURE 12
ZVS waveforms of S_2 under **(A)** light load; **(B)** heavy load.

inductor current iLk indicates that the voltage-matched condition is achieved. The waveforms of the currents are consistent with the theoretical analysis when input voltage varies.

The ZVS waveforms of S_a under 250 V input voltage and different loads are shown in Figure 9. The drain–source voltage across S_a, the driving signal of S_a, the buck inductor current, and the DAB leakage inductor current are shown in the figure. As can be seen, drain–source voltage across S_a has dropped to zero before the driving signal arises. As shown in the experimental results, S_a of the buck stage realizes ZVS under 250 V input voltage at both light and heavy loads. The heavy load condition is 1,000 W, and the light load condition is 300 W.

The ZVS waveforms of S_a under 450 V input voltage and different loads are shown in Figure 10. The drain–source voltage across S_a, the driving signal of S_a, the buck inductor current, and the DAB leakage inductor current are shown in the figure. As can be seen, the drain–source voltage across S_a has dropped to zero before the driving signal arises. As shown in the experimental results, S_a of the buck stage realizes ZVS under 450 V at both light and heavy loads.

The ZVS waveforms of S_1 under both light and heavy loads are shown in Figure 11. The drain–source voltage across S_1, the driving

signal of S_1, the buck inductor current, and the DAB leakage inductor current are shown in the figure. As can be seen, the drain–source voltage across S_1 has dropped to zero before the driving signal arises. As shown in the experimental results, S_1 of the DAB stage realizes ZVS under a wide voltage range at both light and heavy loads.

The ZVS waveforms of S_2 under both light and heavy loads are shown in Figure 12. As can be seen, the drain–source voltage across S_2 has dropped to zero before the driving signal arises. As shown in the experimental results, S_2 of the DAB stage realizes ZVS under a wide voltage range at both light and heavy loads.

The experimental results of bidirectional power transfer are shown in Figure 13. As can be seen, under forward power transmission mode, the phase of u_{ab} is ahead of the phase of u_{cd}, as shown in Figure 13A. In addition, under backward power transmission mode, the phase of u_{ab} lags behind the phase of u_{cd}, as shown in Figure 13B.

The measured efficiency comparisons of the proposed MBDAB converter and the TSBDAB converter are shown in Figure 14. It includes experimental results under different loads and different input voltages. To ensure the fairness of comparison, the input and output voltage and the circuit parameters of the DAB circuit of the TSBDAB converter are
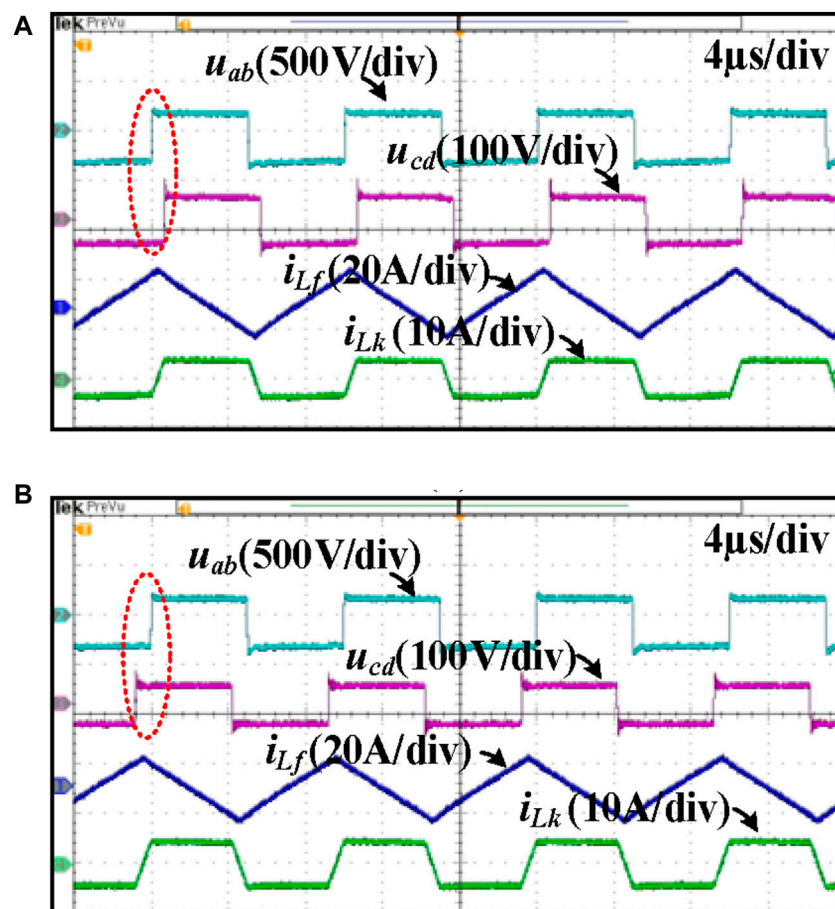
FIGURE 13
Bidirectional waveforms under 1,000 W: **(A)** forward mode; **(B)** backward mode.

the same as the MBDAB converter. In addition, to make a comparison under the same magnetic component, the inductance of the buck inductor in the TSBDAB converter is also designed the same as that in the MBDAB converter. This means that the ZVS condition of the buck part cannot be achieved under some load conditions in the TSBDAB converter. At lower input voltage, the proposed MBDAB converter has a higher efficiency than buck-DAB under a full-load range due to the partial power transmission characteristic. At medium input voltage, the two converters have similar efficiencies due to the similar current of i_{Lf}. At higher voltage, the proposed MBDAB converter has a higher efficiency than the buck-DAB converter due to the lower inductor current.
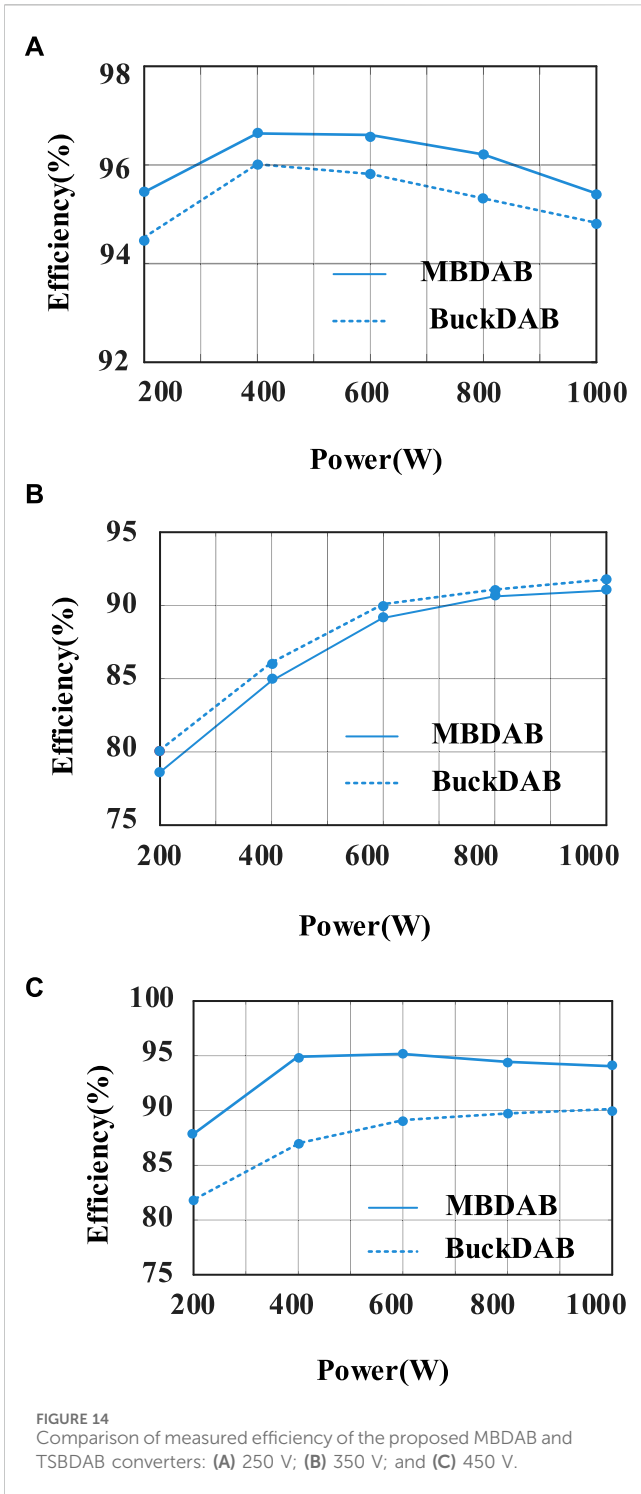
The loss breakdown of the proposed MBDAB converter under different input voltages and different loads is shown in Figure 15. The C3M0045065D of CREE is adopted as the MOSFETs of the primary and secondary switches of the converter. The PQ40-40 and RM10 are used as the inductor and transformer core of DAB. In addition, the inductor type of buck used for the prototype is Kool Mμ Toroid of 77071A7.

As shown in the figure, the total loss of the MBDAB converter under 350 V input voltage is higher than that of

the input voltages at 250 V and 450 V, which is mainly caused by the increased inductor L_f iron loss. The peak-to-peak and RMS values of the buck inductor current under this operating point are larger. In addition, it can be seen from Figure 13 that the estimated efficiency is basically consistent with the measured efficiency with slightly mismatching. For example, at the output power of 200 W, the estimated losses are 9.4 W, 41.5 W, and 17.8 W at the input voltages of 250 V, 350 V, and 450 V, which are close to the measured efficiencies of 95.3%, 79.2%, and 91.1%, respectively.
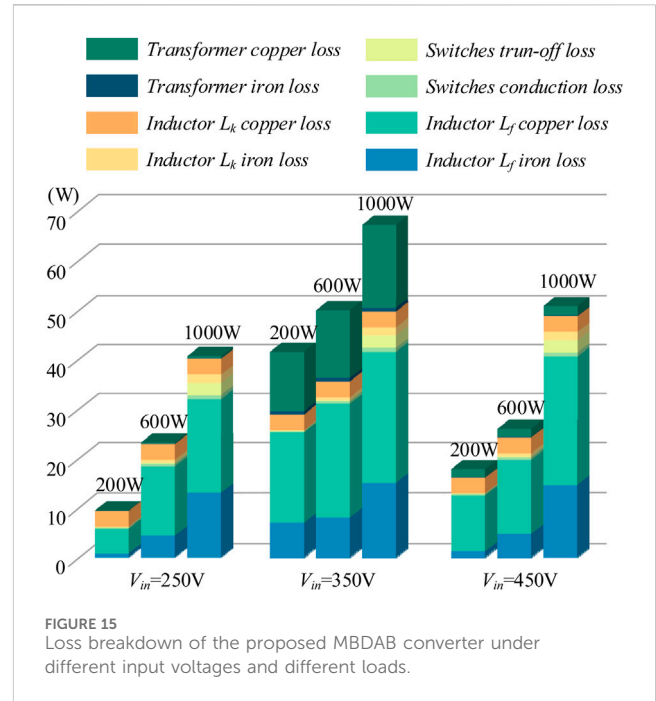
5 Conclusion

In this article, a modified two-stage isolated bidirectional buck-DAB converter is proposed. When the input voltage of the MBDAB changes, the front-end buck stage performs gain adjustment, whereas DAB operates under a fixed voltage gain condition. The buck stage can only transmit part of the output power, which is due to the change in the TSBDAB scheme. All the switches of the proposed converter can achieve the ZVS condition. Working principle, voltage gain ratio analysis, power transfer

FIGURE 14
Comparison of measured efficiency of the proposed MBDAB and TSBDAB converters: **(A)** 250 V; **(B)** 350 V; and **(C)** 450 V.

FIGURE 15
Loss breakdown of the proposed MBDAB converter under different input voltages and different loads.

characteristic, and ZVS analysis are introduced for the MBDAB converter.

The experimental results show that the proposed MBDAB converter can realize partial power transmission of the buck stage and ZVS of all switches, which reduces losses of the MBDAB converter effectively.

Data availability statement

The raw data supporting the conclusions of this article will be made available by the authors, without undue reservation.

Author contributions

JL: software and writing–original draft. DW: investigation and writing–review and editing. ZL: methodology and writing–review and editing. GX: validation and writing–review and editing.

Funding

Conflict of interest

Authors JL and DW were employed by State Grid Hunan Electric Power Company Limited Research.

The remaining authors declare that the research was conducted in the absence of any commercial or financial relationships that could be construed as a potential conflict of interest.

The authors declare that this study received funding from State Grid Hunan Electric Power Company Limited. The funder had the following involvement in the study:Thesis preparation, theoretical analysis and design.

Publisher's note

All claims expressed in this article are solely those of the authors and do not necessarily represent those of their affiliated organizations, or those of the publisher, the editors, and the reviewers. Any product that may be evaluated in this article, or claim that may be made by its manufacturer, is not guaranteed or endorsed by the publisher.

References

Alou, P., Oliver, J., and Cobos, J. A. (2001) "Buck + half bridge (d = 50%) topology applied to very low voltage power converters," in Annual IEEE Applied Power Electronics Conference and Exposition (APEC).

Doncker, R. W. D., Divan, D. M., and Kheraluwala, M. H. (1988). "A three-phase soft-switched high power density dc/dc converter for high power ap-plications," in Conference Record of the 1988 IEEE Industry Applications Society Annual Meeting, January-February, 1991 (IEEE), 1, 796–805.

Everts, J. (2017). Closed-form solution for efficient ZVS modulation of DAB converters. *IEEE Trans. Power Electron.* 32 (10), 7561–7576. doi:10.1109/tpel.2016.2633507

Fu, M., Fei, C., Lee, F. C., and Li, Q. (2020). A GaN-based DC–DC module for railway applications: design consideration and high-frequency digital control. *IEEE Trans. Ind. Electron.* 67 (2), 1638–1647. doi:10.1109/tie.2019.2896279

Guo, Z. (2020). Modulation scheme of dual active bridge converter for seamless transitions in multi-working modes compromising ZVS and conduction loss. *IEEE Trans. Ind. Electron.* 67 (9), 7399–7409. doi:10.1109/tie.2019.2945270

Inoue, S., and Akagi, H. (2007). A bidirectional DC–DC converter for an energy storage system with galvanic isolation. *IEEE Trans. Power Electron.* 22 (6), 2299–2306. doi:10.1109/tpel.2007.909248

Lee, J., Jeong, Y., and Han, B. (2011). An isolated DC/DC converter using high-frequency unregulated LLC resonant converter for fuel cell applications. *IEEE Trans. Ind. Electron.* 58 (7), 2926–2934. doi:10.1109/tie.2010.2076311

Liao, Y., Xu, G., Peng, T., Sun, Y., Yang, Y., and Xiong, W. (2022). Power-estimation-Based synchronous rectification solution for bidirectional DAB-LLC converter. *IEEE Trans. Circuits Syst. II Express Briefs* 69 (3), 1213–1217. doi:10.1109/TCSII.2021.3104884

Lin, N., Zhao, Z., Diao, F., Zhao, Y., and Balda, J. C. (2022). A current-fed dual-half-bridge-based composite converter with improved light-load efficiency through a multi-variable optimization. *IEEE Trans. Transp. Electrification* 8 (2), 3008–3020. doi:10.1109/tte.2021.3126726

Masrur, M. A., Skowronska, A. G., Hancock, J., Kolhoff, S. W., McGrew, D. Z., Vandiver, J. C., et al. (2018). Military-based vehicle-to-grid and vehicle-to-vehicle microgrid—system architecture and implementation. *IEEE Trans. Transp. Electrific* 4 (1), 157–171. doi:10.1109/tte.2017.2779268

Shao, S., Chen, H., Wu, X., Zhang, J., and Sheng, K. (2019). Circulating current and zvs-on of a dual active bridge dc-dc converter: a review. *IEEE Access* 7, 50 561–650 572. doi:10.1109/access.2019.2911009

Sun, J., Sun, Q., and Wang, P. (2020). Improved dynamic response strategy with dual phase-shift control for dual-active-bridge DC-DC converter. *IET Power Electron.* 13 (12), 2671–2674. doi:10.1049/iet-pel.2020.0076

Sun, J., Xu, M., Reusch, D., and Lee, F. C. (2008). "High efficiency quasi-parallel voltage regulators," in Proc. 23rd annu. IEEE appl. Power electron. Conf. Expo, Austin, TX, USA, February 24–28, 2008 (IEEE), 811–817.

Tu, H., Feng, H., Srdic, S., and Lukic, S. (2019). Extreme fast charging of electric vehicles: a technology overview. *IEEE Trans. Transp. Electrific* 5 (4), 861–878. doi:10.1109/tte.2019.2958709

Xu, C., Liu, S., and Guo, X. (2020) "A novel converter integrating buck-boost and DAB converter for wide input voltage," in The 46th Annual Conference of the IEEE Industrial Electronics Society (IECON), Singapore, October 18–21, 2020 (IEEE).

Zhao, B., Song, Q., Liu, W., and Sun, Y. (2014). Overview of dual-active-bridge isolated bidirectional DC–DC converter for high-frequency-link pow-er-conversion system. *IEEE Trans. Power Electron.* 29 (8), 4091–4106. doi:10.1109/tpel.2013.2289913

Zhao, B., Yu, Q., and Sun, W. (2012). Extended-phase-shift control of isolated bidirectional DC-DC converter for power distribution in microgrid. *IEEE Trans. Power Electron.* 27 (11), 4667–4680. doi:10.1109/tpel.2011.2180928

Zientarski, J. R. R., da Silva Martins, M. L., Pinheiro, J. R., and Hey, H. L. (2019). Evaluation of power processing in series-connected partial-power converters. *IEEE J. Emerg. Sel. Top. Power Electron.* 7 (1), 343–352. doi:10.1109/jestpe.2018.2869370